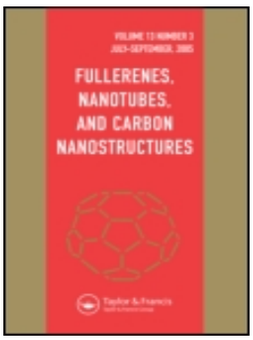

Fullerenes, Nanotubes and Carbon Nanostructures

ISSN: 1536-383X (Print) 1536-4046 (Online) Journal homepage: http://www.tandfonline.com/loi/lfnn20

Study on micro-patterning process of vertically aligned carbon nanotubes (VACNTs)

M. R. Mohd Asyraf, M. Masud Rana, T. Saleh, Harrison D. E. Fan, Andrew T. Koch, Alireza Nojeh, Kenichi Takahata & A. B. Suriani

To cite this article: M. R. Mohd Asyraf, M. Masud Rana, T. Saleh, Harrison D. E. Fan, Andrew T. Koch, Alireza Nojeh, Kenichi Takahata & A. B. Suriani (2016) Study on micro-patterning process of vertically aligned carbon nanotubes (VACNTs), Fullerenes, Nanotubes and Carbon Nanostructures, 24:2, 88-99, DOI: 10.1080/1536383X.2015.1119126

To link to this article: http://dx.doi.org/10.1080/1536383X.2015.1119126

Accepted author version posted online: 30 Nov 2015.
Published online: 30 Nov 2015.

FULLERENES, NANOTUBES AND CARBON NANOSTRUCTURES
2016, VOL. 24, NO. 2, 88–99
http://dx.doi.org/10.1080/1536383X.2015.1119126

Taylor & Francis
Taylor & Francis Group

Study on micro-patterning process of vertically aligned carbon nanotubes (VACNTs)

M. R. Mohd Asyraf[a], M. Masud Rana[a], T. Saleh[a], Harrison D. E. Fan[c], Andrew T. Koch[c], Alireza Nojeh[c], Kenichi Takahata[c], and A. B. Suriani[b]

[a]Smart Structures, Systems and Control Research Laboratory (S3C RL), Faculty of Engineering, Department of Mechatronics Engineering, International Islamic University Malaysia, Kuala Lumpur, Malaysia; [b]Faculty of Science and Mathematics, Department of Physics, Universiti Pendidikan Sultan Idris, Tanjung Malim, Perak, Malaysia; [c]Department of Electrical and Computer Engineering, University of British Columbia, Vancouver, BC, Canada

ABSTRACT

Vertically aligned carbon nanotubes (VACNTs) have drawn significant attention by the researchers because of their nanometric size and favorable material properties. Patterning of CNT forests in the micrometric domain is very important for their application in the area of microelectromechanical system (MEMS). For the first time this paper reports, detailed experimental investigation on a post growth μ-patterning process of VACNT forests. The micromechanical bending (M2B) process was locally applied at the targeted area in order to change the alignment of VACNT forests. Interestingly, the VACNT forest was transformed from typical black body absorber to reflective mirror as the M2B process was applied. Several parameters were identified that govern the resultant patterns such as rotational spindle speed, lateral bending speed, step size, tool morphology, and total depth of bend. Optimization of the parameters was carried out experimentally to obtain the best surface roughness and integrity of the microstructure. A minimum average surface roughness of Ra = 15 nm was achieved with 2000 rpm spindle speed, 1 mm/min bending speed and 1 μm step size.

ARTICLE HISTORY
Received 13 October 2015
Accepted 9 November 2015

KEYWORDS
Carbon nanotubes; micromechanical bending; MEMS; 3-DMicro fabrication

Introduction

Carbon nanotube (CNT) has attracted interest from researchers around the world, owing to its fascinating physical (1), electrical (2), optical (3) and thermal properties (4). Vertically aligned carbon nanotubes array generally termed as CNT forests are also being considered to be embedded as part of microelectromechanical systems (MEMS) and nanoelectromechanical systems (NEMS) (5). Some of the engineering applications where CNTs are used as reported are, solar cells (6), cooling fins (7), field emitters (8), strain sensors (9), gas sensors (10) and biological applications (11). Scientists have been working hard in various areas related to CNT forest which covers synthesis, post-growth processing and implementation as part of the nanodevices. However, as discussed by Jariwala et al. (12), limited application and commercialization of Carbon Nano Material throughout society is partially due to lack of precision assembly and structural inhomogeneity. Therefore, post growth micropatterning process is important for CNT forest to achieve 3-D structures on bare VACNT array with desirable accuracy and precision.

There is a list of techniques to perform micro-patterning, each with its own merits. Rubio et al. (13) introduced an electron beam to cut the CNTs, but the method is limited to an individual CNT. Lim et al. (14) used a laser to shape various CNT-based structures, but the approach lacked accuracy and control due to thermal damage. Zhu et al. (15) used arc discharge to pattern some shapes on bare MWCNT (multiwalled carbon nanotubes array) array; however, an arc is less controlled due to high energy thus less accurate. Arc discharge is replaced by spark discharge in micro-electro-discharge machining (μEDM) (16) for structural modification of CNT forests as reported by Khalid et al. (17), however, it still inherited spark gap problems to some degree. Then, Saleh et al. (18) improved this technique, first by reversing the polarities of the tool and workpiece, being this time such that the CNT forest is the cathode while the tool is the anode, taking advantage of the CNTs as a good field emitter. After that, the improvement effort was continued by the same author (19) by replacing the ambient air with high dielectric gas SF6. In order to upscale the production, Sarwar et al. (20) proposed batch mode μ-EDM operation for patterning CNT forest. In spite of significant efforts made by various researchers on μ-EDM based patterning process of VACNT array the problems of spark gap or clearance tolerances still exist.

Structural modification using the micromechanical bending (M2B) method is different from μEDM in term of mechanism and concept. μEDM uses spark energy to remove the material by oxygen plasma etching while M2B is solely a mechanical treatment on the CNT forest to shape the pattern, even though both techniques use a rotating tool to pattern CNT forests. In M2B process, the tool rotates and moves in a plane with a certain depth to bend and flatten the vertical CNTs. After controlled repetition of the tool motion, a resultant structure can be formed on the bare CNT forest. To the best of authors'

CONTACT T. Saleh tanveers@iium.edu.my Faculty of Engineering, Department of Mechatronics Engineering, International Islamic University Malaysia, PO BOX 10, Kuala Lumpur, 50728, Malaysia.
Color versions of one or more of the figures in the article can be found online at www.tandfonline.com/lfnn.

knowledge, there is no detailed study which has been carried out on the M2B method that could be useful on the micropatterning process of CNT forests. This μ-processing technique of CNT forest may open the opportunity of using VACNTs array as a micro-optical switch, flexible memory chips, position encoders and other types of MEMS devices. In this report, the method of M2B has been investigated in-depth to examine its characteristics. M2B is purely a mechanical processing of CNT forest, which bends and entangles bundle of CNTs to follow the direction of tool movement. Various parameters were assessed and the optimal parameter set was identified. The effects of various tools with different surface topography were also examined. Finally, the optimal parameter was applied to make various shapes and forms of 3-D structures, to show its feasibility for micron domain applications. This study reveals the potential advantages of micromechanical bending of CNT forest over other patterning processes in terms of tolerance gap (between the tool and resultant structure), process controllability and surface finish.

Experimental procedure

CNT forest preparation

The CNT forest samples were prepared using an atmospheric-pressure chemical vapor deposition (CVD) system, on highly doped silicon substrates (<100> n-type, resistivity 0.008–0.015 Ωcm). Al and Fe of 10 and 2 nm, respectively, in thickness, were used as catalysts for the growth. The growths were conducted by flowing the gases (ethylene, hydrogen and argon) at certain ratios and temperature. The details of the preparation process with specific conditions has been demonstrated by Khalid et al. (17). Vertically aligned multi-walled CNT array (100's of μm height) was fabricated with areas in the order of cm^2 using the process demonstrated by Khalid et al. (17).

Micro-mechanical bending (M2B) process

The M2B experiments were performed using a servo-controlled 3-axis Micro-CNC system (Mikrotools Ltd) with the capability of 1 μm positioning resolution. First, the tool was positioned just above the CNT forest while rotated at a defined speed. The μtool (made of tungsten) was fabricated with a predefined diameter using a method called wire electro discharge grinding (WEDG). Various capacitances and voltages of machining were used in this purpose (the process concept was introduced by Masuzawa et al. (21)). Then, the μtool was programmed to move downward in the Z direction with a defined step size before moving in the lateral (X and Y) directions. Step size could be described as the distance in the Z direction taken by the μtool in each round of scanning. This technique would create a pattern on the VACNT array by the local mechanical manipulation of the CNTs. Figure 1 illustrates original VACNTs and patterning processes using the M2B method. The tool was rotated at various spindle rotational speeds during all the patterning conditions. The lateral speed of the motion in X–Y directions and the tool step increment in the Z direction were also varied. Table 1 below summarizes all the patterning parameters. Experiments were repeated three times to ensure consistency and the average value was reported with error bar.

Initially, nine experiments were conducted (with three times repetitions) by varying the spindle speed and step size in the Z direction for patterning CNT forest. The resultant structures were all characterized in order to determine the optimal

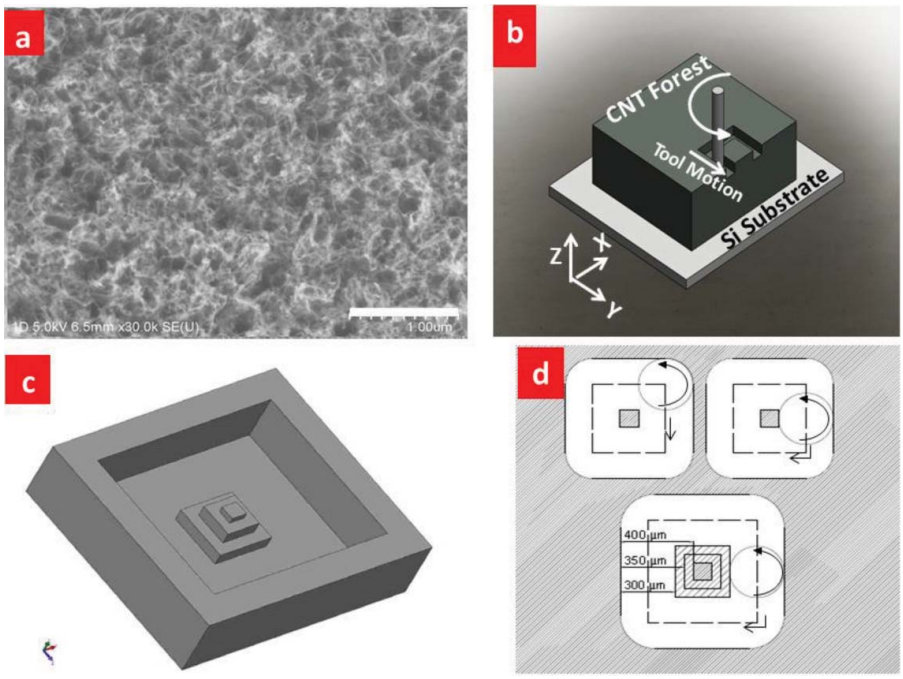

Figure 1. (a) Field Emission Scanning Electron Microscopy of original VACNTs. Scale bar, 3 μm. (b) the concept of M2B method. The tool is rotated while moving in the X and Y directions in each round, before moving in the Z direction. (c) 3-D model of the planned mini pyramid pattern. (d) Top view of the square pattern in an orbit size 0.4 mm $\times$ 0.4 mm and planned mini pyramid pattern.

Table 1. M2B Method conditions used for μ-processing of CNT forest.

Rotational Spindle Speed (rpm)	1000, 1500, 2000
Lateral speed in the *X*–*Y* directions (mm/min)	1, 5, 10
Step size in the *Z*-direction (μm)	1, 5, 10
Total depth (μm)	60, 100, 300
Tool material	Tungsten
Tool size, diameter (μm)	300
Tool machining condition with WEDG	Tool 1—90 V, 0; (stray capacitance was 13 pF) Tool 2—100 V, 10 nF; Tool 3—110 V, 0.4 μF.

parameters which produced the smoothest surface. In the next phase, lateral speed was further varied at 5 mm/min and 10 mm/min to see its effect. Subsequently, the best set of parameters was employed to pattern at various total depths of 60 μm, 100 μm, and 300 μm. To see the impact of different tool topography on the CNT forests, three dissimilar tools were fabricated using larger discharge energy by increasing the voltage and capacitance. Lastly, the best parameter set was employed to construct various 3-D structures to reveal micro-patterning feasibility.

Experimental characterization and measurement

To evaluate the surface roughness of the resultant square patterns, XE-100 AFM (Atomic Force Microscopy) was used with a scan rate of 0.2 Hz over the area of 10 μm × 10 μm. The relative optical reflectance of the bent CNT forests was measured using an Olympus optical microscope with model number BX-141, which was calculated by comparing the highest brightness of the pattern with the rest, so the brightest pattern was designated at 100%. Raman spectra characterization was also carried out for the mechanically bent forest and original bare forest using a Renishaw in Via Raman microscope. A Renishaw in Via Reflex Raman spectroscopy equipment with a He-Ne laser source (632.8 nm, 2 mW) was utilized, and the incident beam was focused on the targeted area in a backscattering geometry through a 50× objective lens(N.A. = 0.8), forming a sample spot of approximately 2 μm in diameter. Morphological analysis of bent forest structures was performed using a scanning electron microscope (SEM) with an energy-dispersive X-ray (EDX) spectroscopic analyzer (Hitachi S-3000 N).

Results and discussion

As the tool was rotated while moving towards the CNT forest to bend and flatten the nanotubes, the originally super black material's surface became smoother and reflective. This top-down structural modification of the bare CNT forest could compress and bend individual CNTs or bundles of CNTs in the direction of the tool motion. Bare CNT forests are highly porous materials with a porosity value of more than 92% (22). After the process, hollow space will be covered as the CNTs are compacted, thus surface porosity will be significantly reduced. In this study, it was observed that different parameters will result in different levels of surface roughness and reflectivity.

Study of surface roughness and morphology

Surface roughness is an important consideration for the M2B method since it will affect the reflectivity of the bent surface (23). Very smooth surfaces will reflect light concentrated around the specular angle of reflectance, and the surface will appear mirror-like and glossy. Thus, specular reflection is preferred for achieving higher reflection and having high contrast reflector-absorber array for potential applications such as optical encoders. Low surface roughness or smooth surfaces are also desirable for good patterning integrity and maintaining crack free structures of CNT forests. Figure 2(a) shows surface topography of the smoothest pattern (average surface roughness R_a = 15 nm) as measured by Atomic Force Microscopy (AFM).

Effect of tool rotation speed

The tool's rotation speed is an important consideration that has a direct impact on the surface roughness. The CNT forest is very spongy, fragile and sensitive to the touch; even a very small force could transform the structure of CNT forests. Too low a tool rotation speed would cause the CNTs to dislodge with respect to each other and not compacted properly, as discussed by Razib et al. (24). They also mentioned that too high a tool rotation speed would cause cracks to appear on the flattened area, caused by spindle vibration related to machine limitations. An optimized tool rotation speed is required to achieve smoothest and lowest value of surface roughness. As shown in (Figure 2a and b), the best value of surface roughness was obtained to be 15 nm (Ra) with 2000 rpm and 1 μm step size. It can also be observed from (Figure 2b) that variation of the tool rotation speed in a range of 1000 rpm–2000 rpm did not have a significant effect on the surface finish of the flattened area. However, it had an effect on the integrity of the resultant structure. For example for a step size of 5 μm, crack propagation on the sidewall and on the resultant square island at lower rpm patterning (1000 rpm) was more visible as compared to that of 2000 rpm (Figure 2c and d), though the value of the average surface roughness was lower for 1000 rpm than 2000 rpm. This observed phenomenon can be explained as follows. It can be seen from (Figure 1a) that VACNTs are not truly vertical and there is a significant gap between CNTs because of porosity. Therefore, higher spindle rotation pushed CNTs (caused by centrifugal force) towards the sidewalls hence aligned them which could not be fully achieved with low spindle speed. Therefore, narrow crack was observed both on the inner island and on the sidewall (Figure 2c). Machine limitations also played a factor to determine the best tool rotation speed, in this case, the bearing and motor capacity. At speeds higher than 2000 rpm, vibration from the spindle could occur (judging from the noise noticed from the bearing) and thus might have caused the tool to start to wobble and reduce the precision. Also, as reported by Razib et al. (24), cracks start to occur on the flattened area at 2500 rpm. Overall, 2000 rpm was found to be the optimal tool rotational speed to pattern the CNT forests.

Effect of step size

Step size is the depth taken in the *Z* direction during each cycle of motion in the *X*–*Y* plane. A high value of step size

will result in a larger CNT portion being bent downward in the Z direction while rotated (for example 10 μm step size compresses more compared to 1 μm step size). From the graph in (Figure 2b), different step sizes give random readings of surface roughness with no obvious trend. Thus, it is suggested that within step size tested (1 μm–10 μm), it does not have a notable effect on the surface roughness. However, when studying the FE-SEM images of the pattern (Figure 2e–f), it was found that step size of 10 μm produced cracks in the side wall and island areas (square cube at the centre), with cracks shown in the red mark box. Patterns with 1 μm step size on the other hand (Figure 2a, g and h), had sharper edges with smooth surfaces. A possible reason behind this observation could be same as the reason stated for tool rotational speed. When the tool tried to bend bulk of CNTs with a larger step size few CNTs could not be compacted together and aligned with the side walls that eventually caused the crack. Once the sidewall starts to crack, it is likely to propagate to the flattened area of the structure which, in the long run, will cause the side wall to collapse for deeper patterns. Therefore, it is concluded from this experiment that the optimal step size is 1 μm.

Effect of lateral bending speed

Reduced processing time means savings in production costs. The effort of reducing processing time must not sacrifice the quality, in this case, surface roughness. Lateral bending speed influences the processing time and quality. Too high a lateral bending speed (>25 mm/min) would result in the lesser time required to pattern but would deteriorate the surface quality (24). This study further narrowed down the parameter of lateral bending speed to the 1 mm/min–10 mm/min range. It was observed that a 1 mm/min speed produces the best surface roughness with Ra = 15 nm which was ~ 2 × better than 5 mm/min or 10 mm/min sample (Figure 3a). Both 5 mm/min and 10 mm/min parameters produced a bad surface on the sample, however, surface roughness achieved by 10 mm/min lateral bending speed was slightly (~27%) better than that of 5 mm/min speed. On the contrary to surface roughness their morphology study (Figure 3b and c) suggest that the 10 mm/min pattern started to exhibit side wall and island crack because fast moving tool could not have enough time to push and compact individual CNTs effectively towards the wall. Further, when the speed reached 25 mm/min, the crack became

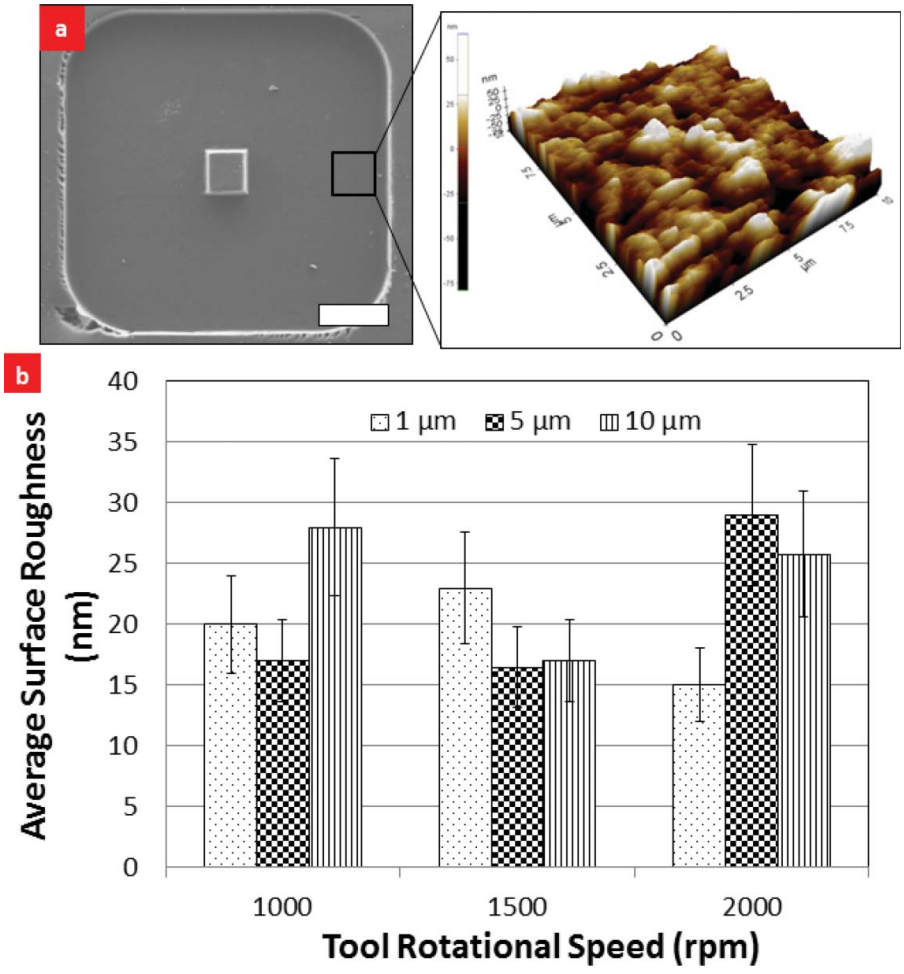

Figure 2. (a) AFM result of the surface shows high quality surface finish with R_a15 nm with 2000 rpm, 1 mm/min speed, and 1 μm step size. Scale bar, 150 μm. (b) Average surface roughness at different spindle rotation speeds, rpm (with constant lateral speed 1 mm/min). (c–h) Field emission scanning electron microscopy (FE-SEM) image of patterns with different parameters as stated in the figure. The red box shows cracks starting to build up at the edge of the side wall. Scale bar for the zoom in pictures are 100 μm and rest are 150 μm.

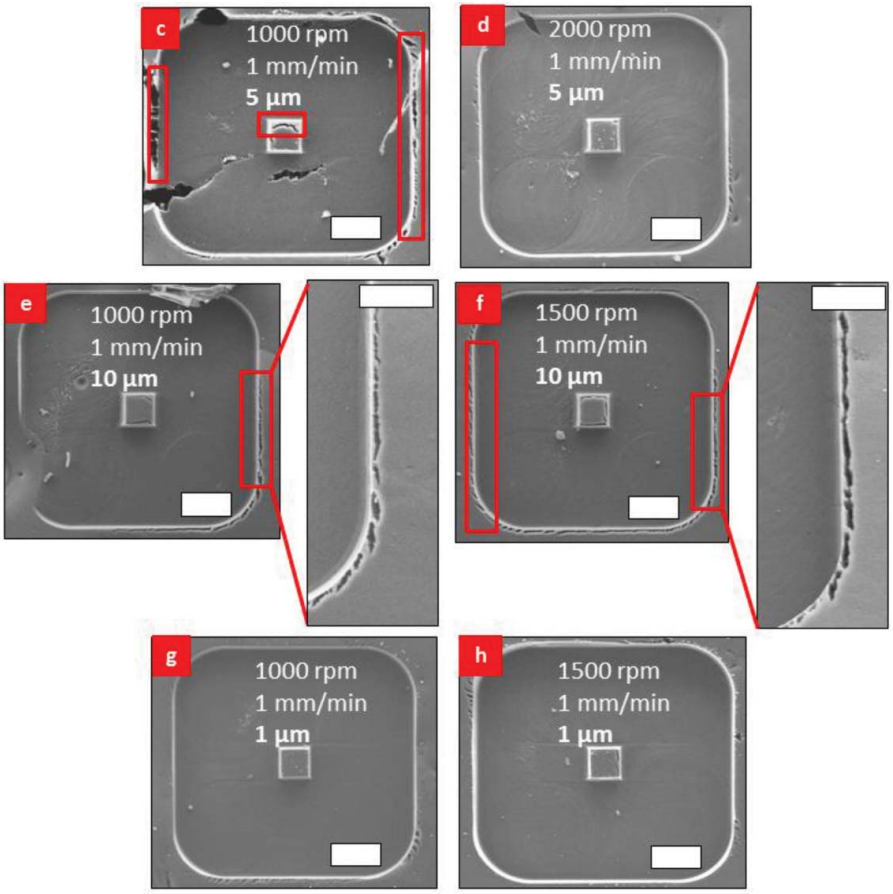

Figure 2. (Continued)

predominant and propagated into the flattened CNT zone (24), which was quite distinct.

Effect of tool topography

The tool is formed by machining the tungsten rod to the intended size using wire electro-discharge grinding (WEDG) with specific voltage and capacitance values. Morgan et al. (25) showed that different voltage and capacitance values would produce different types of tool topography, which may have different impacts on the surface roughness of the bent region. This study has compared three types of tools which were produced by three sets of discharge energy: (1) 90 V, 0 F (stray capacitance = 13 pF), (2) 100 V, 10 nF, and (3) 110 V, 0.4 μF, which correspond to increasing the value of discharge energy to form the tool. (Figure 4a) shows the varieties of discharge energy to produce the tool against the average surface roughness. Theoretically, low discharge energy will produce a finer tool, thus smoother surface on the bent CNT region. While tool no.1 (90 V, 13 pF) and tool no.2 (100 V, 10 nF) showed good agreement with theory, tool no.3 (110 V, 0.4 μF) showed a slightly different result, which has lower surface roughness value as compared to tool no.2. It is clear from (Figure 4c) and (Figure 4d) that tool no.3 (110 V, 0.4 μF) produced less visible circular tool marks as compared to tool no.2 (100 V, 10 nF). A possible reason behind this could be as follows. Figure 4c shows that there are some regions where tool did not touch the CNT surface (due to unevenness on original CNT forest topography) and that indicates CNTs were not bent and flattened enough to produce smoother surface hence higher surface roughness value compared to (Figure 4d). Furthermore, it was also observed that tool 2 and tool 3 produced smaller middle islands (thus affecting the tolerance) as shown in (Figure 4c and d), which might have also resulted from the coarse surface of tool no.2 and tool no.3.

Effect of tool motion

Many attempts have been made to control the direction and arrangement of grown CNT forests, which is known to be vertical from the substrate surface. B.Q. Wei et al. (26) used a direction controlled chemical vapour deposition (CVD) method to assemble CNTs in different pre-set orientation onto silicon/silica substrates. Lu and Chen (27) demonstrated the use of mechanical shearing on the composite membranes of aligned Single Wall Carbon Nanotubes (SWCNTs) to control the orientation direction.

CNTs processed with M2B technique will bend individual CNTs by following the resultant vector of rotational and lateral motion as shown in (Figure 5a and b). The resultant tool path was generated by the highest point on the tool surface located at a distance r from the centre. As the tool was rotated and moved linearly, the circular path was traced by the point P (P1 to P2) as described in (Figure 5a and b). The tracing point's X and Y coordinates can be determined as follows. To determine the x-coordinate of point P2 (after time t), the distance

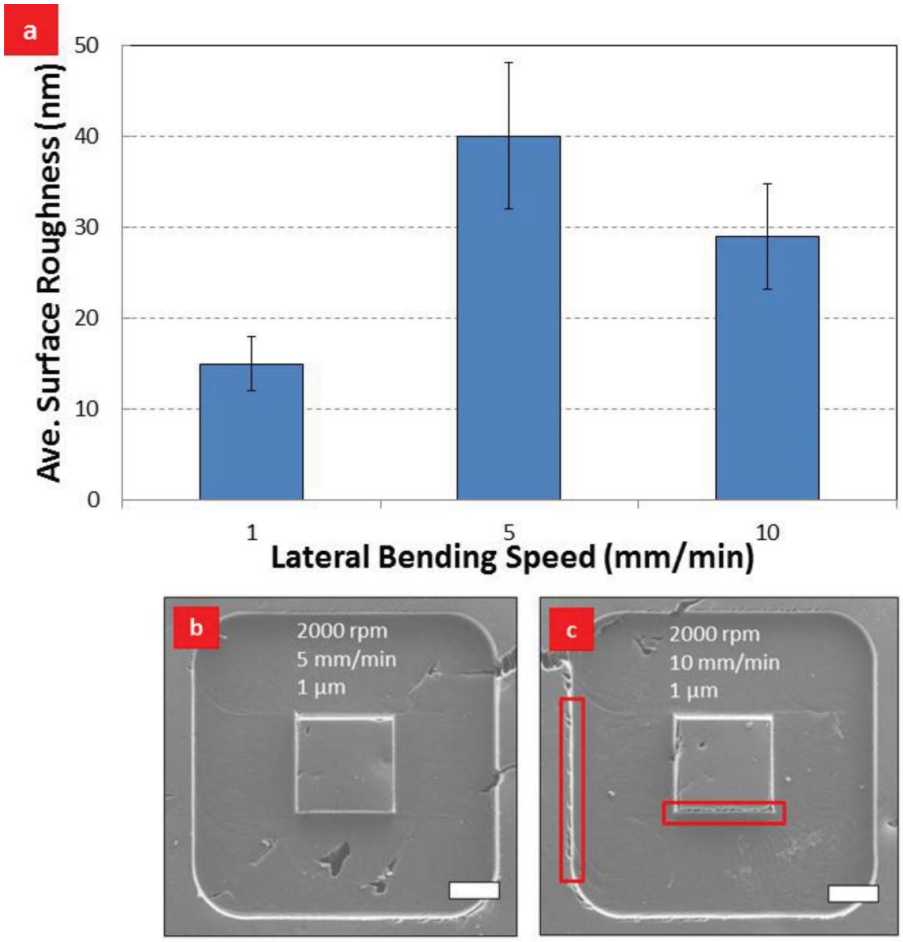

Figure 3. (a) Graph of average surface roughness against various lateral bending speeds. (b) & (c) FE-SEM image of pattern with parameters differing in lateral bending speed at 5 mm/min and 10 mm/min, respectively. Scale bar, 150 μm.

travelled in the x direction is $X = \mathrm{OP} = \mathrm{OA–PB}$. OA is the distance the circle rolled to the right, or vt, where v is velocity and t is time travelled. From triangle PCB (Figure 5a): PB = r (sin ωt). Hence, X = vt − r (sin ωt).To determine the y-coordinate of point P2 (after time t), the "height" of point P is Y = BA = CA–CB. We know that CA = r. From triangle PCB (Figure 5a), CB = $r\cos\theta$. Hence, Y = r (1 − cos ωt).Therefore, tool marks on the CNT forest can be modeled by the equation:

$$X = vt - r(\sin\omega t), \tag{1}$$

$$Y = r(1 - \cos\omega t), \tag{2}$$

where X = lateral distance travelled in the x-direction (mm); Y = lateral distance travelled in the y-direction (mm); v = lateral bending speed in the x-direction (mm/min); t = time travelled (seconds); r = radius of the tool (mm); ω = angular speed (rad/sec)

In order to determine the distance between two tool marks D, following procedures can be followed. D can be found by subtracting adjacent two X coordinates when corresponding Y coordinates are equal to the radius of the tool, i.e. 0.15 mm in this case. Hence,

$$D = X2 - X1, \quad \text{where} \quad (Y2 = Y1 = r). \tag{3}$$

Now, Y2 = Y1 = r = r (1 − cos ωt).

Therefore, $t = \frac{\eta\pi}{2\omega}$, where n = 1,3,5,7…

To determine D two times value would be, $t_1 = \frac{\eta\pi}{2\omega}$ and $t_2 = \frac{(n+4)\pi}{2\omega}$ as depicted in (Figure 5a). Finally D could be written as follows:

$$D = X2 - X1 = vt2 - r(\sin\omega t\,2) - vt1 + r(\sin\omega t\,1)$$

$$= v(t2 - t1) - r(\sin\omega t\,2 - \sin\omega t\,1). \tag{4}$$

Figure 5c shows a comparison between simulated value of D (using equation 4) and experimental value of D for a constant v (1 mm/min).

Study of reflectivity

Reflectivity is a function of electromagnetic radiation wavelength, λ and surface roughness root mean square RMS, σ. As defined by the Rayleigh criterion, a surface behaves as a smooth surface as long as the surface RMS (σ) is very small relative to

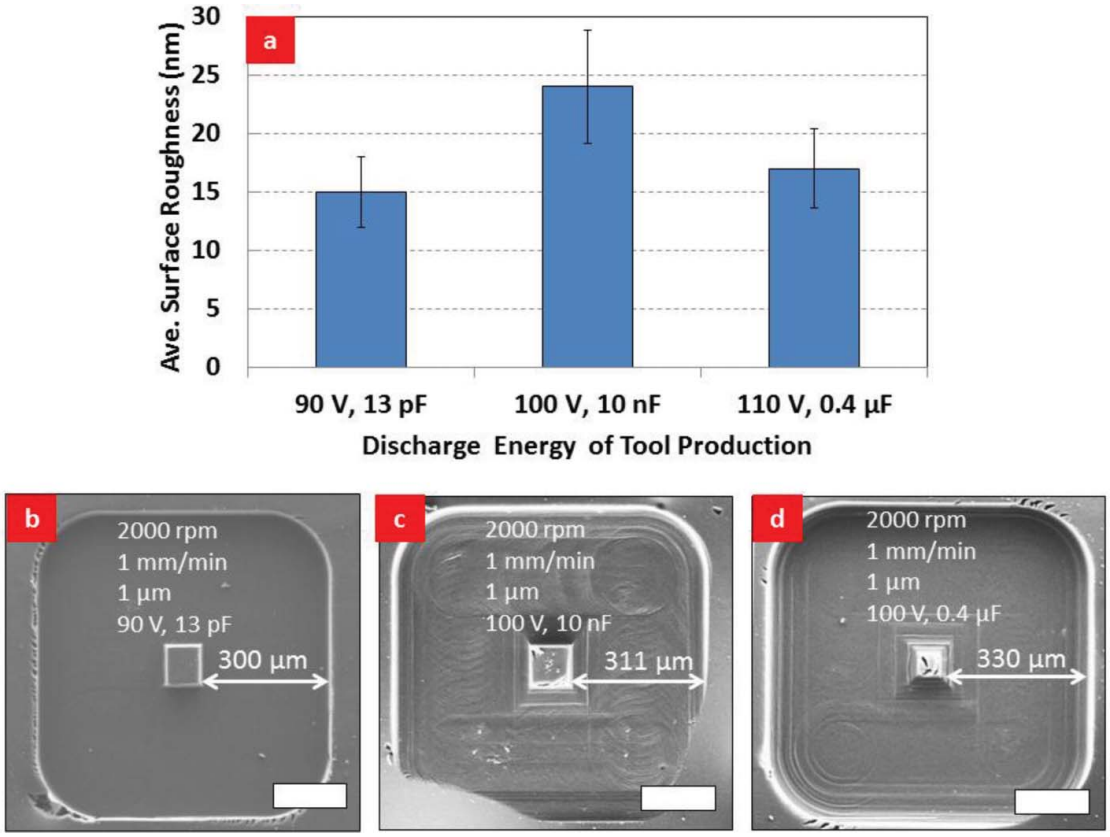

Figure 4. (a) Graph average surface roughness against various discharge energies of tool production. (b–d) FE-SEM image of shape pattern with parameters written on the image. Scale bar, 150 μm.

the wavelength (λ), which is $\sigma/\lambda << 1$. Oppositely, if $\sigma/\lambda > 1$, then the surface behaves as a rough or matte surface. Smooth surfaces could produce good reflection, as good as optical quality. It was observed in the study that specular reflectivity has a direct relationship with the surface roughness. Optical microscopy was used with constant magnification to measure the relative reflectance by measuring and comparing the brightness of the image. The value of reflectance was normalized against the patterned sample with the highest brightness (i.e. patterns created at spindle speed 2000 rpm, step size of 1 μm and bending speed 1 mm/min, resulting in a surface roughness of 15 nm). Figure 6a describes the relationship between surface roughness and optical reflectivity: there is a trend that as the Ra value becomes higher, reflectivity becomes lower. This is well in line with the previous study by Yonehara et al. (28). In contrast, low surface roughness, due to fewer peaks and valleys on the surface of the bent region, resulted in a reflectivity as good as optical quality. Further it was also observed that if there is any crack in the patterned zone that opens up the porous CNT region, it would behave like a black body absorber as described in (Figure 6b–c). Crack would open up space for light to enter CNT forests thus extinguished due to multiple reflections and absorption by the CNTs inside the forests (Figure 6d). This multiple reflection follows geometric progression as explained below:

$$a_n = ar^n, \tag{5}$$

where a_n is output optical power coming out of the CNT forest after multiple reflections and an incident optical power, r is reflectance of individual nanotubes and n is the number of reflection. The reflectance of individual nanotube could be taken as 15% (29). After first and second reflection, the reflectance will be reduced to 15% and 2.25% accordingly (Figure 6e) and eventually output optical power will progress to zero if there are several internal reflections before it comes out of the forest as shown in (Figure 6d) and (Figure 6e). That is the reason why cracked region of CNTs behaved as a black body absorber as shown in (Figure 6c).

Raman spectroscopy analysis

In order to understand how the proposed patterning process induces stress into the bended CNT zone, Raman spectroscopy study was carried out. (Figure 7a) shows that Raman shift for G band (I_g) is increased as the depths of the pattern areas are increased. A similar case was reported by Sandler et al. (30), where the author investigated the effect of applied compressive pressure on CNTs by using Raman spectroscopy. It was observed that G band peak was shifted due to the stress induced by the mechanical force imparted on the CNTs due to applied hydraulic pressure. Similarly, as the total depth of patterns increases, more residual compressive stress is induced on the patterned CNT forest and the G band shift increased (Figure 7a). With the purpose of testing the limit of M2B process, three different aspect ratio structures were patterned. In all cases, the programmed dimensions of the inner islands were maintained constant but only the depth of the patterns

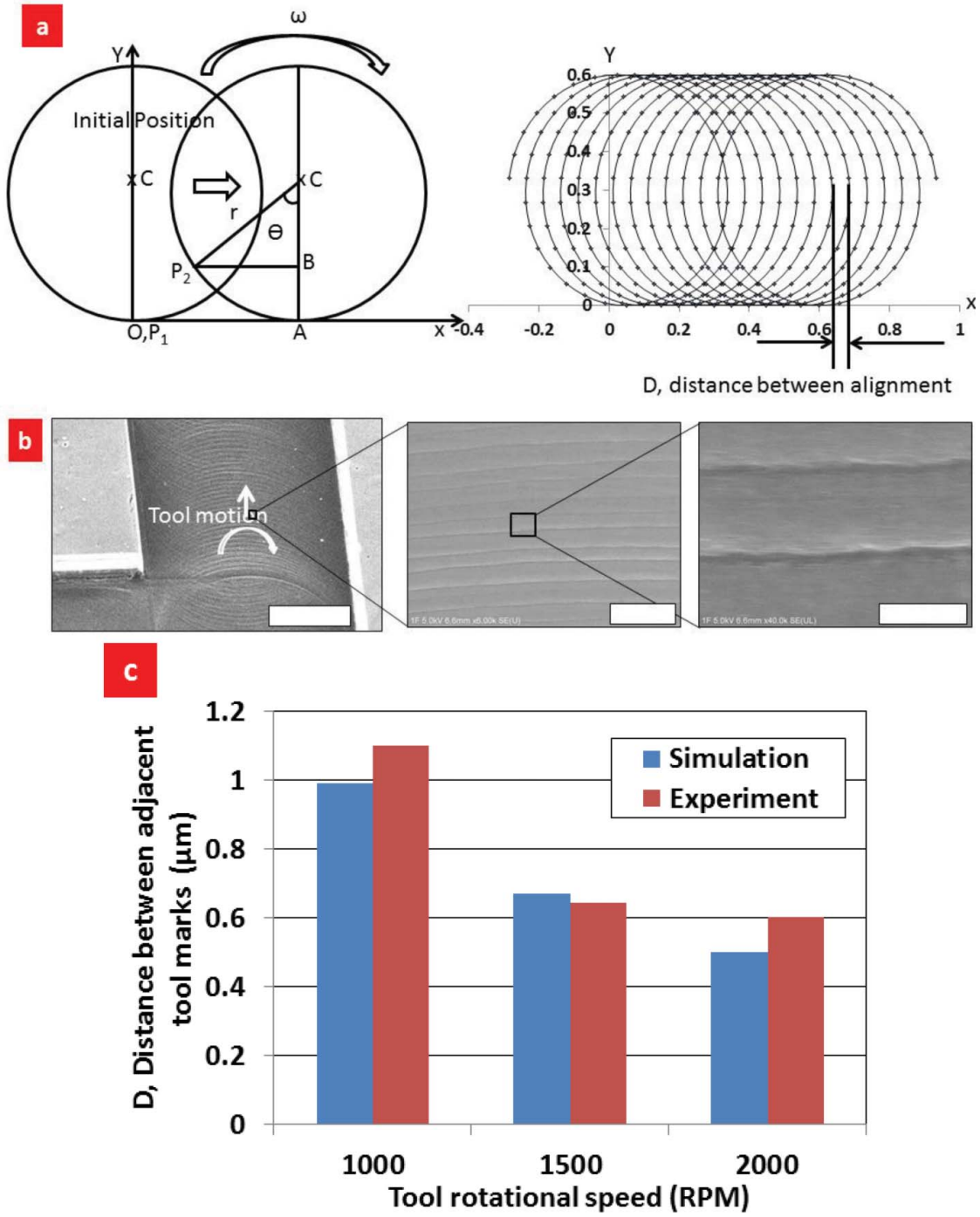

Figure 5. (a) On the left, shows position of the tracing point *P* after time *t*, on the right, schematic diagram of circular tool motion. (b) High-resolution FE-SEM images are showing the tool marks on the bent CNT region, with parameters of 1000 rpm and 1 mm/min. Left, middle, and right picture scale bar are 150 μm, 5 μm, and 1 μm, respectively. (c) Graph of D, distance D against tool rotational speed (RPM). All lateral bending speed is maintained at 1 mm/min.

were varied. The figure shows that integrity of the islands remained intact until 100 μm of depth (Figure 7b) and (Figure 7c). As the depth of the pattern was increased the inner island collapses (Figure 7d) due to excessive residual stress.

Energy dispersive X-ray spectroscopy (EDX)

Finally, the energy dispersive X-ray spectroscopy (EDX) analysis (Figure 8) of the processed CNT zone shows predominantly Carbon with some trace of silicon. The source of Si was mainly from the substrate. Tungsten, the tool material, was not detected, suggesting that the M2B method involved zero consumption of the tool and thus did not cause contamination of the material on the surface. It is because, as mentioned before, the process is purely of mechanical type treatment in nature on the CNT forests and does not have any impact on the integrity of the tool. The result is consistent with the previous study by Razib et al. (24) and Saleh et al. (29).

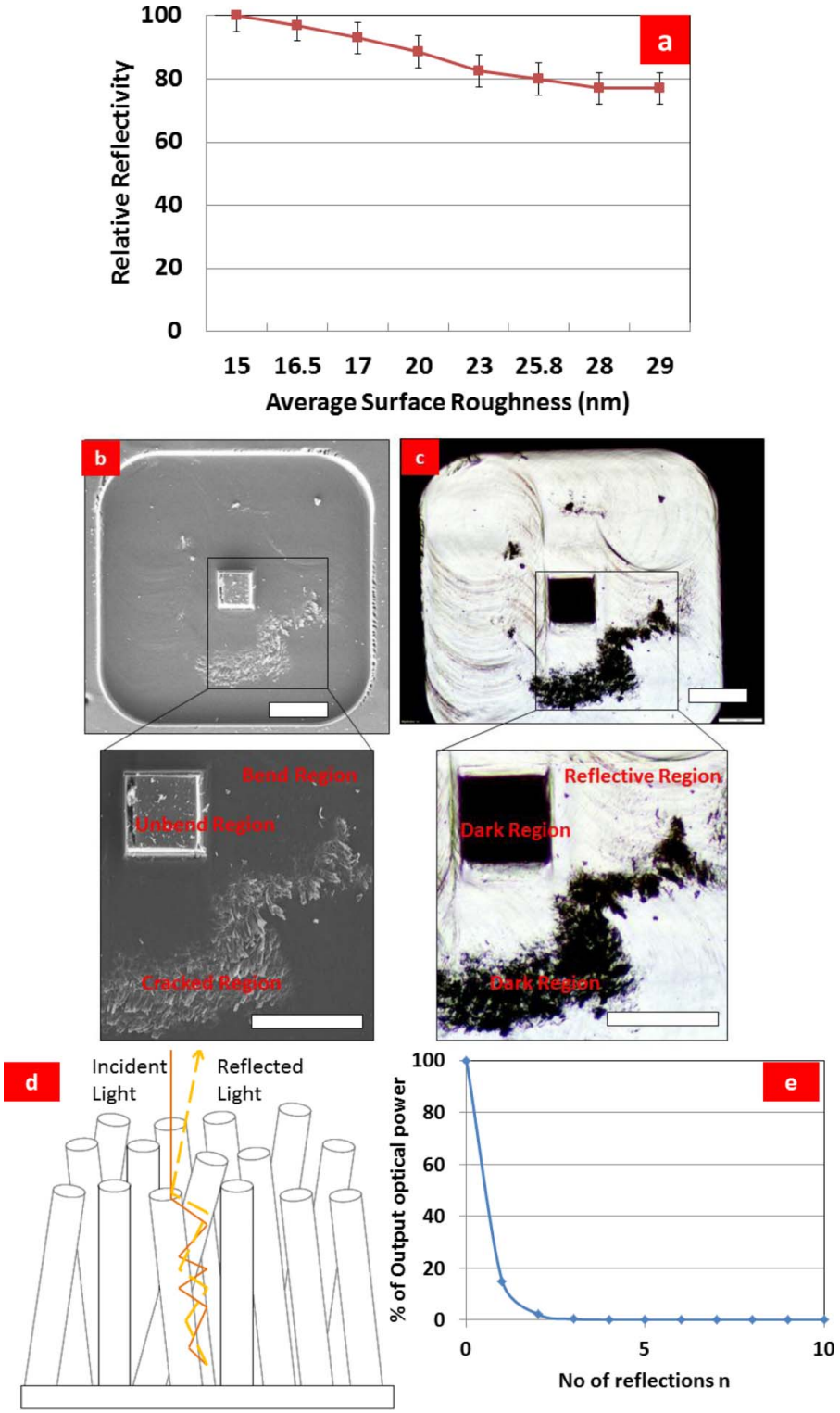

Figure 6. (a) Graph of relative reflectivity versus average surface roughness: as the average surface roughness, R_a (nm) increases, relative reflectance will decreases. (b–c) FE-SEM and optical image of patterns created by M2B method and resultant cracked area on the processed area. Scale bars, 150 μm. (e) Graph of reflected optical power from CNT forest against number of internal reflection shows how reflectance of CNT forest will be dramatically reduced as the number of internal reflections are increased.

Example of microstructures and applications

It is challenging to fabricate microstructures with good structural integrity and nanometric surface roughness on CNT forest. Many researchers have attempted various techniques as described in the introduction. Here, M2B method was used to fabricate various types of structures on the CNT forest to show the process capability. Some examples are shown in (Figure 9) such as mini-pyramid, IIUM letters and micro-tower. The fabricated CNT pyramid proves that the process is capable of maintaining micro step resolution on the resultant structure. The mini-towers produced (Figure 9b) has an aspect ratio of 2 with 50 μm width and 100 μm heights. (Figure 9c–f) show letter patterns on CNT forest and concurrent existence of optically dark and reflective area on the same material. This

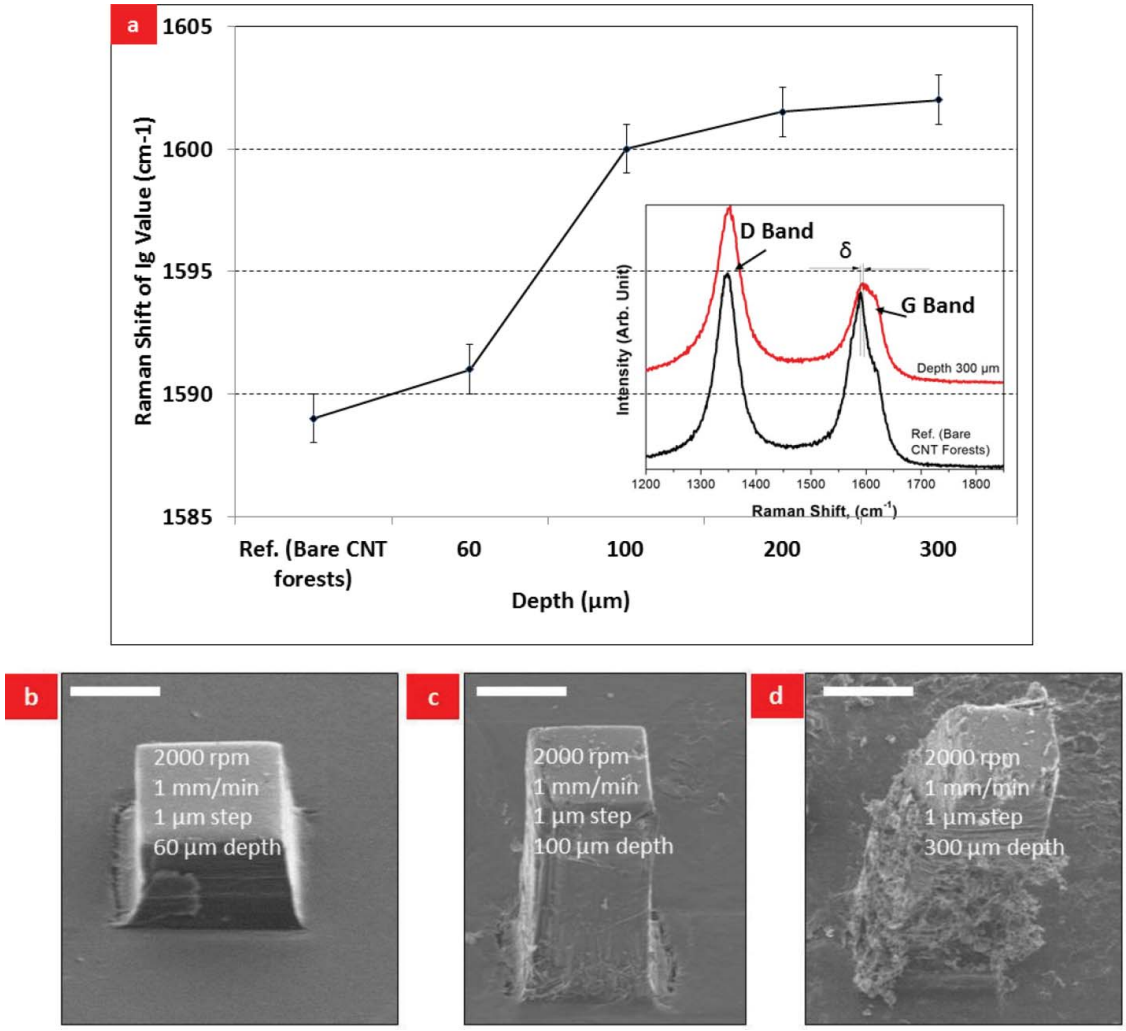

Figure 7. (a) Surface characterization of the bent CNT pattern using Raman Spectroscopy shows increasing value of I_g shift as total depth of pattern increases, suggesting that as the depth increases, surface stress also increases. Field emission of scanning electron microscopy (FE-SEM) of pattern, with parameters of 2000 rpm, 1 mm/min speed, and 1 μm step size. (b) 60 μm depth, (c) 100 μm depth, and (d) 300 μm depth. Scale bar is 50 μm.

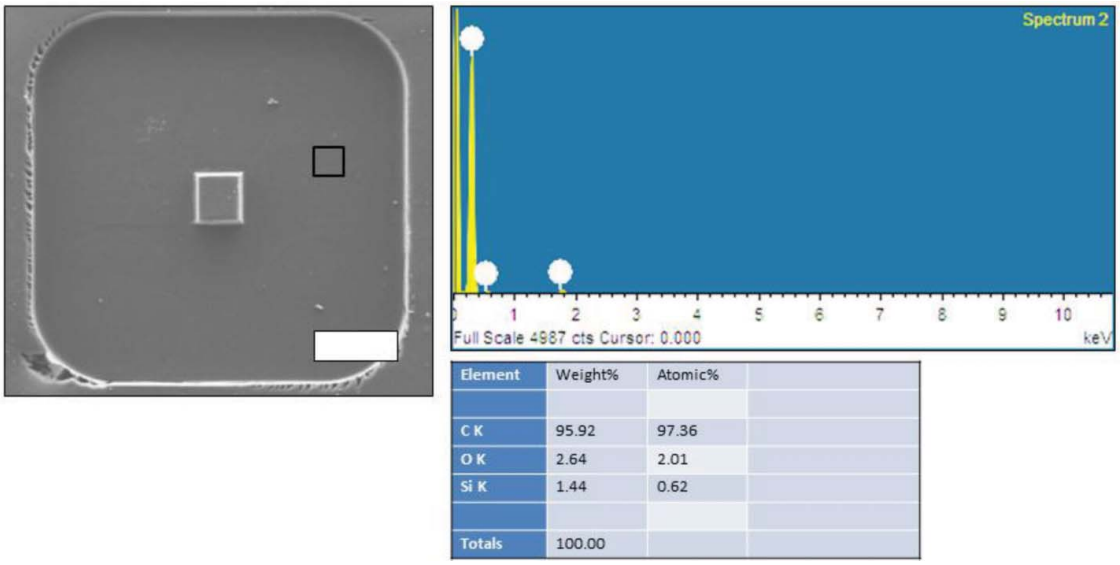

Figure 8. (a) Surface of the bent CNT pattern characterized by EDX Spectroscopy. Reading is taken from the small black box area in left FE-SEM image. FE-SEM image of a pattern of bent CNTs with a result from EDX, suggesting that there is only carbon, trace of silicon and oxygen present on the surface of the processed region. All reading from different patterns resulted in similar results. Scale bar, 150 μm.

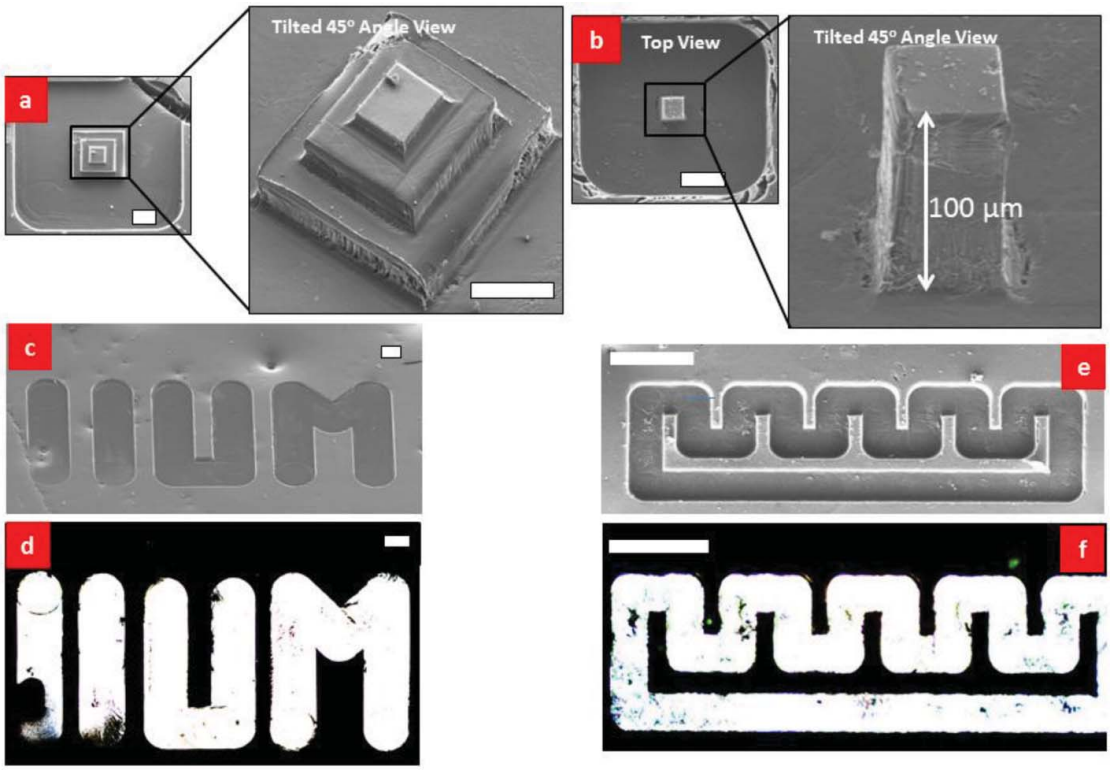

Figure 9. (a) Pyramid structure pattern on the grown CNT forest. Scale bar, 150 μm. (b) Mini tower with aspect ratio of 2. Scale bar, 150 μm. (c) & (d) FE-SEM image of IIUM pattern and optical reflectivity on the CNT forest. Scale bar, 150 μm. (e) & (f) FE-SEM and optical image alternating super dark absorber material and reflector. Scale bar, 150 μm.

property is useful and could be exploited to develop CNT-based flexible position encoder as shown in (Figure 9f). Further, alternative arrays of dark absorber and mirror reflector of CNT forest can be used as optical switches which would be useful for fiber optic communications (Figure 9d and f).

Conclusion

In this paper, top down micro-patterning using the Micro-Mechanical Bending (M2B) technique of CVD grown VACNT/CNT forests was investigated. This method of VACNT patterning has the potential to eliminate spark gap problem associated with μ-EDM-based patterning process. Therefore, this post-processing technique of CNT forest could enhance significantly the resolution of the resultant structures. A detailed characterization of M2B process was carried out for the first time to investigate the effect of different parameters on the method. Following salient points can be concluded from the study.

1. It was observed that higher rotational speed of the spindle with low step size in the Z direction and low lateral speed (X & Y directions) could produce μ-patterns on CNT forest with good structural integrity and surface finish. Too high spindle speed (>2000 RPM) degrades the pattern quality due to excessive vibration. On the other hand low spindle speed, higher step size in the Z direction and higher lateral speed (X & Y directions) adversely affect the integrity of the structure as the processing tool cannot compact and align VACNTs with the sidewalls that eventually caused cracks.
2. M2B process drastically reformed the optical property of VACNT from dark absorber to reflective mirror. Surface roughness was observed to be the key factor in governing the reflectance from the processed CNT zone. Therefore, highest optical reflectance from bended CNT zone was achieved with the optimized parameters with tool rotational speed at 2000 RPM, lateral speed at 1 mm/min and Z-directional step size 1 μm.
3. It was observed that as the depth of pattern was increased the residual stress on the surface also increased, which was confirmed by studying the shift of the peak of G band in Raman spectroscopy on the processed CNT zone. This excessive stress caused the deeper pattern to collapse.
4. EDX study on the processed zone confirmed that patterns produced by the proposed M2B method are free from contamination of the tool, which is a significant advantage over μ-EDM based patterning of CNT forest.
5. This process will be suitable for making use of patterned VACNT arrays in various engineering applications such as a micro-optical switch (by making an alternative array of the dark absorber and mirror reflector on same material (Figure 9d and f), calibration patterns for high-end instruments like AFM (alternative grating structures as shown in (Figure 5b). Moreover, reflective nanotubes on the patterned area are flexible, they will be useful in flexible memory chips based on optics. Patches of bent nanotubes area (which are reflective) could represent 1 s and absorbing erect ones 0 s and light can be used to read out the data.

Acknowledgments

Authors are very grateful to IIUM, UPSI, UiTM, and MIMOS for providing machining and testing facilities to carry out the experiments and all their valuable support to carry out this research work.

Funding

This work was financially supported by MOSTI (SF14-008-0058) and MOHE (FRGS13-083-0324). K. Takahata is supported by the Canada Research Chairs program.

References

1. Kashyap, K. T., and Patil, R. G. (2008) On Young's Modulus of multi-walled carbon nanotubes. *Bull. Mater. Sci.*, 31(2): 185–187.
2. Park, M., Cola, B. A., Siegmund, T., Xu, J., Maschmann, M. R., Fisher, T. S., and Kim, H. (2006) Effects of a carbon nanotube layer on electrical contact resistance between copper substrates. *Nanotechnology*, 17 (9): 2294–2303.
3. Tooski, S. B., Godarzi, A., Solari, M. S., Ramyar, M., and Roohforouz, A. (2011) Optical properties of carbon nanotube gas sensor. *J. Appl. Phys.*, 110(3): 034307.
4. Berber, S., Kwon, Y. K., and Tománek, D. (2000) Unusually high thermal conductivity of Carbon Nanotubes. *Phys. Rev. Lett.*, 84(20): 4613–4616.
5. Hierold, C., Jungen, A., Stampfer, C., and Helbling , Nano, T. (2007) Nano electromechanical sensors based on carbon nanotubes. *Sensors Actuators, A Phys.*, 136: 51–61.
6. Klinger, C., Patel, Y., and Postma, H. W. C. (2012) Carbon nanotube solar cells. *PLoS One*, 7(5): e37806.
7. Fu, Y., Nabiollahi, N., Wang, T., Wang, S., Hu, Z., Carlberg, B., Zhang, Y., Wang, X., and Liu, J. (2012) A complete carbon-nanotube-based on-chip cooling solution with very high heat dissipation capacity. *Nanotechnology*, 23(4): 045304.
8. Saito, Y., and Uemura, S. (2000) Field emission from carbon nanotubes and its application to electron sources, *Carbon N. Y.*, 38(2): 169–182.
9. Qiu, W., Li, S. L., Deng, W. L., Gao, D., and Kang, Y. L. (2014) Strain sensor of carbon nanotubes in microscale: From model to metrology. *Sci. World J.*, 2014.
10. Savu, R., Silveira, J. V., Alaferdov, A., Joanni, E., Gobbi, A. L., Canesqui, M. A., de Lara, D. S., Souza Filho, A. G., and Moshkalev, S. A. (2015) Gas sensors based on locally heated multiwall carbon nanotubes decorated with metal nanoparticles. *Carbon Nanotub.*, 1: 60–68.
11. Mundra, R. V., Wu, X., Sauer, J., Dordick, J. S., and Kane, R. S. (2014) Nanotubes in biological applications. *Curr. Opin. Biotechnol.*, 28(1): 25–32.
12. Jariwala, D., Sangwan, V. K., Lauhon, L. J., Marks, T. J., and Hersam, M. C. (2013) Carbon nanomaterials for electronics, optoelectronics, photovoltaics, and sensing. *Chem. Soc. Rev.*, 42: 2824–60.
13. Rubio, A., Apell, S. P., Venema, L. C., and Dekker, C., (2000) A mechanism for cutting carbon nanotubes with a scanning tunneling microscope. *Eur. Phys. J. B 17*, 308: 301–308.
14. Lim, K. Y., Sow, C. H., Lin, Jianyi, Cheong, F. C., Shen, Z. X., Thong, J. T. L., Chin, K. C., and Wee, A. T. S. (2003) Laser pruning of carbon nanotubes as a route to static and movable structures. *Adv. Mater.*, 15: 300–303.
15. Zhu, Y. W., Sow, C. H., Sim, M. C., Sharma, G., and Kripesh, V. (2007) Scanning localized arc discharge lithography for the fabrication of microstructures made of carbon nanotubes. *Nanotechnology*, 18(38): 385304.
16. Saleh, T., Rasheed, A. N., and Muthalif, A. G. (2015) Experimental study on improving μ-WEDM and μ-EDM of doped silicon by temporary metallic coating. *Int. J. Adv. Manuf. Technol.*, 78(9–12): 1651–1663.
17. Khalid, W., Ali, M. S. M., Dahmardeh, M., Choi, Y., Yaghoobi, P., Nojeh, A., and Takahata, K. (2010) High-aspect-ratio, free-form patterning of carbon nanotube forests using micro-electro-discharge machining. *Diam. Relat. Mater.*, 19(11): 1405–1410.
18. Saleh, T., Dahmardeh, M., Bsoul, A., Nojeh, A., and Takahata, K. (2011) Field-emission-assisted approach to dry micro-electro-discharge machining of carbon-nanotube forests. *J. Appl. Phys.*, 110(10): 103305.
19. Saleh, T., Dahmardeh, M., Nojeh, A., and Takahata, K. (2013) Dry micro-electro-discharge machining of carbon-nanotube forests using sulphur-hexafluoride. *Carbon N. Y.*, 52: 288–295.
20. Sarwar, M. S. U., Dahmardeh, M., Nojeh, A., and Takahata, K. (2014) Batch-mode micropatterning of carbon nanotube forests using UV-LIGA assisted micro-electro-discharge machining. *J. Mater. Process. Technol.*, 214(11): 2537–2544.
21. Masuzawa, T., Fujino, M., Kobayashi, K., Suzuki, T., and Kinoshita, N. (1985) Wire electro-discharge grinding for micro-machining. *CIRP Ann.—Manuf. Technol.*, 34(1): 431–434.
22. Puretzky, A. A., Geohegan, D. B., Jesse, S., Ivanov, I. N., and Eres, G. (2005) In situ measurements and modeling of carbon nanotube array growth kinetics during chemical vapor deposition. *Appl. Phys. A*, 81: 223–240.
23. Saleh, T. (2013) μ-patterning of carbon nanotube (CNT) forest for MEMS applications. *IOP Conf. Ser. Mater. Sci. Eng.*, 53: 012050.
24. M Razib, M. A. , and Saleh, T., M. H. (2014) Micro-mechanical bending (M2B) method for carbon nanotube (CNT) based sensor fabrication. *Smart Instrumentation, Measurement and Applications (ICSIMA), 2014 IEEE International Conference on IEEE* 25–27.
25. Morgan, C., Shreve, S., and Vallance, R. R. (2003) Precision of micro shafts machined with wire electro-discharge grinding. *Proceedings of the Winter Topical Meeting on Machines and Processes for Micro-Scale and Meso-Scale Fabrication, Metrology, and Assembly. American Society for Precision Engineering (ASPE)*, 28: 26–31.
26. Wei, B. Q., Vajtai, R., Jung, Y., Ward, J., Zhang, R., Ramanath, G., and Ajayan P. M. (2002) Organized assembly of carbon nanotubes. *Nature*, 495–496.
27. Lu L., and Chen, W. (2010) Large-scale aligned carbon nanotubes suspension. *ACS Nano*, 4(2): 1042–1048.
28. Yonehara, M., Matsui, T., Kihara, K., Isono, H., Kijima, A., and Sugibayashi, T. (2004) Experimental relationships between surface roughness, glossiness and color of chromatic colored metals. *Mater. Trans.*, 45(4): 1027–1032.
29. Saleh, T., Moghaddam, M. V., Mohamed Ali, M. S., Dahmardeh, M., Foell, C. A., Nojeh, A., and Takahata, K. (2012) Transforming carbon nanotube forest from darkest absorber to reflective mirror. *Appl. Phys. Lett.*, 101(6): 061913.
30. Sandler, J., Shaffer, M., Windle, A., Halsall, M., Montes-Morán, M., Cooper, C., and Young, R. (2003) Variations in the Raman peak shift as a function of hydrostatic pressure for various carbon nanostructures: A simple geometric effect. *Phys. Rev. B*, 67: 1–8.